


Quantum signatures of the topological phase in bosonic quadratic systemsYaohua Li ¹ and Yong-Chun Liu ^{1,2,*}¹*State Key Laboratory of Low-Dimensional Quantum Physics, Department of Physics, Tsinghua University, Beijing 100084, China*²*Frontier Science Center for Quantum Information, Beijing 100084, China*

(Received 26 June 2023; accepted 20 November 2023; published 6 December 2023)

Quantum entanglement and classical topology are two distinct phenomena that are difficult to be connected together. Here we discover that an open bosonic quadratic chain exhibits topology-induced entanglement effect. When the system is in the topological phase, the edge modes can be entangled in the steady state, while no entanglement appears in the trivial phase. This finding is verified through the covariance approach based on the quantum master equations, which provide exact numerical results without truncation process. We also obtain concise approximate analytical results through the quantum Langevin equations, which perfectly agree with the exact numerical results. We show the stationary entanglement originates from the matching between the near-zero eigenenergies of the topological edge states and the system-environment coupling (denoted by the dissipation rate). Our work reveals that the stationary entanglement can be a quantum signature of the topological phase in bosonic systems and, inversely, the topological quadratic systems can be powerful platforms to generate robust entanglement.

DOI: [10.1103/PhysRevA.108.062405](https://doi.org/10.1103/PhysRevA.108.062405)**I. INTRODUCTION**

Quantum entanglement, a key feature of quantum effects, plays an important role in quantum information [1] and quantum metrology [2]. Quantum entanglement allows two distant systems to be correlated with each other, and the measurement results of one system can influence that of the other system, which is in stark contrast to classical physics [3,4]. Nowadays, quantum entanglement has been considered as a major quantum resource to realize quantum computational advantages [5–7]. Moreover, entanglement in atomic ensembles can reduce the quantum noise with enhanced measurement sensitivity [8–16].

In the field of condensed matter physics, long-range entanglement is a signature of the quantum topological phase, which is a property of many-body systems with topological order [17]. On the contrary, the topology widely investigated in ultracold atoms [18–24] and photonic systems [25–32] is indeed classical topology, which originates from the geometric properties of the single-particle wave nature. This kind of topology is characterized by robust edge states or topological invariants and is conventionally believed to be uncorrelated with quantum properties [33].

Parallely, in the field of quantum optics, bosonic quadratic systems, which possess Hamiltonians that are quadratic in terms of bosonic creation and annihilation operators [34], are an important method to generate quantum entanglement [35–37]. The quadratic interactions exist in various platforms, such as bosonic fields with parametrically driving [38–40], interacting Bose-Einstein condensate [41–44], and

optomechanical systems [45,46]. Recently, it is shown that an open quadratic chain exhibits non-Hermitian dynamics [47–50] and novel topology [51–53]. However, the relation between quantum entanglement and topology remains unclear in this system.

Here we uncover the topology-induced entanglement effect in an open bosonic quadratic chain in the steady state. Such an entanglement only emerges between edge modes in the topological phase, while there is no entanglement in the trivial phase, as sketched in Fig. 1. The stationary entanglement is related to the coupling of the system to the environment quantum fluctuations and will be greatly suppressed if the system-environment couplings (denoted by the dissipation rate) do not match the intrasystem couplings (which determines the system eigenenergies). As the absolute values of the eigenenergies of the topological edge states are much smaller than that of the bulk states, it offers the opportunity to match only the topological edge states with the system-environment coupling and thus selectively generate stationary entanglement between the topological edge states. Importantly, this kind of topological matching and related entanglements disappears in the trivial phase when there are no topological edge states. To prove this idea, we approximately solve the Langevin equations by neglecting other eigenenergies except for the near-zero ones of the topological edge states, leading to analytical results, which perfectly match the numerical results obtained from the covariance approach based on the quantum master equations. It is revealed that the emergence of the topological edge states can greatly enhance the squeezing correlations. Our work establishes a relationship between classical topology and quantum entanglements, which sheds new light on the study of quantum topological photonics.

*ycliu@tsinghua.edu.cn

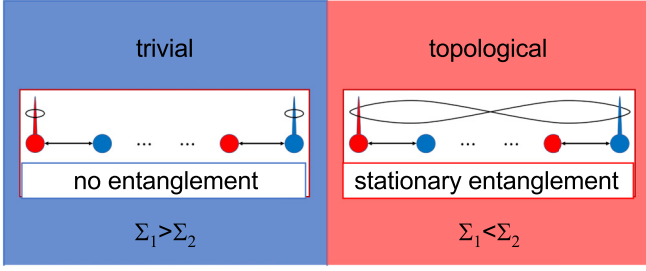


FIG. 1. Stationary entanglement induced by bosonic topology. Phase diagram of the topology and the stationary entanglement with real parameters. The entanglement only emerges in the topological phase, while there is no entanglement in the trivial phase. The equations denote the parameter ranges of the trivial and the topological phases (see definition in Sec. II).

The rest of this work is organized as follows. In Sec. II, we describe the system model of a bosonic quadratic chain and derive the topological phase transition through both the Bloch and non-Bloch band theories. In Sec. III, we analyze the system through the covariance approach based on quantum master equations to obtain exact numerical results. In Sec. IV, we deduce approximate analytical results using the quantum Langevin equations. In Sec. V, we present the analytical results for the quantum behaviors in a two-mode system. In Secs. VI and VII, we describe the quantum behaviors in the trivial and topological phases of the bosonic quadratic chain, respectively. In Sec. VIII, we investigate the topology-induced entanglements between two edge modes. In Sec. IX, we show how to understand the pattern of the logarithmic negativity and maximize the stationary entanglement through the analytical expressions. In Sec. X, we discuss the stationary entanglements with complex-valued coupling strengths. In Sec. XI, we discuss the possible experimental realization. In Sec. XII, we conclude this work with some discussions. In the Appendixes, we provide several parts of the detailed derivations, including the Bloch band theory (Appendix A), the non-Bloch band theory (Appendix B), and the quantum Langevin equations (Appendix C).

II. BOSONIC QUADRATIC CHAIN AND TOPOLOGICAL PHASE TRANSITION

As depicted in Fig. 2(a), we consider a bosonic quadratic chain with both staggered linear interactions and squeezing interactions, which can be viewed as a generalization of the Su-Schrieffer-Heeger (SSH) model [54,55] by adding squeezing interactions. Moreover, we take the system-environment coupling into account by assuming that all the modes are coupled to a Markovian environment with a dissipation rate κ . The system Hamiltonian can be written as ($\hbar = 1$)

$$H = \sum_{j=1}^N (t_1 a_{2j-1}^\dagger a_{2j} + \Delta_1 a_{2j-1}^\dagger a_{2j}^\dagger + \text{H.c.}) + \sum_{j=1}^{N-1} (t_2 a_{2j+1}^\dagger a_{2j} + \Delta_2 a_{2j+1}^\dagger a_{2j}^\dagger + \text{H.c.}), \quad (1)$$

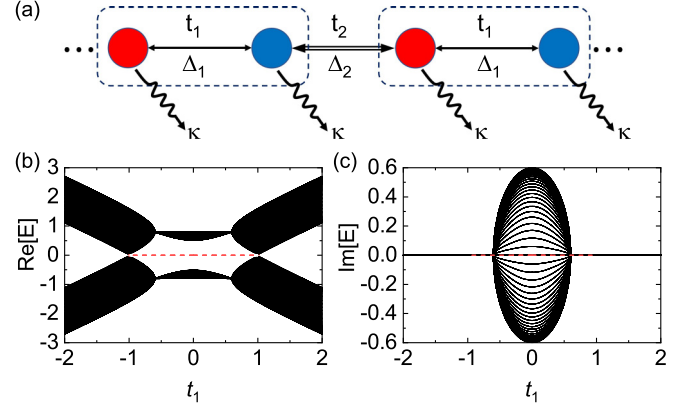


FIG. 2. (a) Bosonic quadratic chain with both staggered linear interactions (t_1, t_2) and squeezing interactions (Δ_1, Δ_2). The dotted boxes indicate the unit cells, and each unit cell contains two bosonic modes. The wavy arrows denote the system-environment couplings described by the dissipation rate κ . (b), (c) The real (b) and imaginary (c) parts of energy spectra for an open chain with length $N = 10$ (unit cell). The red dashed lines indicate the topological edge modes at zero energy. Other parameters are $t_2 = 0.8$, $\Delta_1 = 0.6$, and $\Delta_2 = 0$.

where t_1 (t_2) and Δ_1 (Δ_2) are the intracell (intercell) coupling strengths of linear and squeezing interactions, respectively, N is the number of unit cells, and a_j is the annihilation operator of the j th mode. The Bloch Hamiltonian of the system can be written as

$$\mathcal{H}(k) = (t_1 + t_2 e^{ik}) a_k^\dagger a_k' + (\Delta_1 + \Delta_2 e^{ik}) a_k^\dagger a_{-k}' + \text{H.c.}, \quad (2)$$

or in the matrix form $\mathcal{H}(k) = \frac{1}{2} C_k^\dagger \mathcal{H}_M(k) C_k$, where $C_k^\dagger = (a_k^\dagger, a_k'^\dagger, a_{-k}, a_{-k}')$ (see Appendix A for details). The system satisfies the chiral symmetry, i.e., $\Gamma \mathcal{H}_M \Gamma = -\mathcal{H}_M$ for $\Gamma = \sigma_3 \otimes \sigma_0$, where σ_3 is the third Pauli matrix and σ_0 is the two-dimensional identity matrix.

When the quadratic squeezing terms are nonzero, the excitation modes are no longer unitary transformations of initial bosonic modes. Instead, the excitation modes are Bogoliubov modes that are determined by the eigenvalue equation of $\tau_z \mathcal{H}_M$, where $\tau_z = \text{Diagonal}(\mathbb{1}, -\mathbb{1})$ and $\mathbb{1}$ is an identity matrix with half the dimension of \mathcal{H}_M [48].

Without loss of generality, we assume $t_2 = q_1 t_1 e^{i\phi_1}$, $\Delta_2 = q_\Delta \Delta_1 e^{i\phi_\Delta}$, and $t_1, \Delta_1, q_{t,\Delta}$ are all real. Then the eigenvalues of $\tau_z \mathcal{H}_M(k)$ can be obtained as

$$\xi^2 = \Sigma_1 + \Sigma_2 + 2\Sigma_3 \cos k \pm 2|\sin k| \sqrt{\Sigma_1 \Sigma_2 - \Sigma_3^2}, \quad (3)$$

where $\Sigma_1 = t_1^2 - \Delta_1^2$, $\Sigma_2 = q_1^2 t_1^2 - q_\Delta^2 \Delta_1^2$, and $\Sigma_3 = q_1 \cos \phi_1 t_1^2 - q_\Delta \cos \phi_\Delta \Delta_1^2$. For $\Sigma_1 \Sigma_2 - \Sigma_3^2 \geq 0$, the Bloch spectrum is real, indicating that there is no non-Hermitian skin effect. We can directly obtain the energy spectrum as

$$(\sqrt{\Sigma_1} - \sqrt{\Sigma_2})^2 < \xi^2 < (\sqrt{\Sigma_1} + \sqrt{\Sigma_2})^2, \quad (4)$$

where we assume $\Sigma_{1,2}$ are both positive. When $\Sigma_1 < 0$ or $\Sigma_2 < 0$, the eigenvalues of the long open chain are imaginary, and the system becomes unstable. Consequently, we are only interested in the stable region for $\Sigma_{1,2} > 0$. According to the bulk-edge correspondence, the gap-closing points $\Sigma_1 = \Sigma_2$ ($|t_1|^2 - |\Delta_1|^2 = |t_2|^2 - |\Delta_2|^2$) also denote the gap-closing

points of an open chain and are where the topological phase transition takes place.

However, when $\Sigma_1 \Sigma_2 - \Sigma_3^2 < 0$, the Bloch spectrum forms a loop in the complex energy plane with the emergence of the non-Hermitian skin effect. In this case, the Bloch bulk-edge correspondence fails but can be rebuilt with the non-Bloch theory. The non-Bloch matrix $\mathcal{H}_M(\beta)$ can be obtained from $\mathcal{H}_M(k)$ by the replacements $e^{ik} \rightarrow \beta$, $e^{-ik} \rightarrow \beta^{-1}$ [48], which is

$$\begin{aligned} \mathcal{H}(\beta) = & (t_1 + t_2\beta)a_k^\dagger a'_k + (\Delta_1 + \Delta_2\beta)a_k^\dagger a'_{-k} \\ & + (t_1^* + t_2^*\beta^{-1})a_k a_k'^\dagger + (\Delta_1^* + \Delta_2^*\beta^{-1})a_k a'_{-k}. \end{aligned} \quad (5)$$

The eigenvalues of $\tau_z \mathcal{H}_M(\beta)$ become

$$\begin{aligned} \xi^2 = & \Sigma_1 + \Sigma_2 + \Sigma_3(\beta + \beta^{-1}) \\ & \pm \sqrt{-(\beta - \beta^{-1})^2 \sqrt{\Sigma_1 \Sigma_2 - \Sigma_3^2}}. \end{aligned} \quad (6)$$

We can also obtain the generalized momentum as

$$\beta = \frac{1}{2} \frac{\lambda^2 - \Sigma_1 - \Sigma_2 \pm \sqrt{(\xi^2 - \Sigma_1 - \Sigma_2)^2 - 4\Sigma_1 \Sigma_2}}{\Sigma_3 \pm \sqrt{\Sigma_3^2 - \Sigma_1 \Sigma_2}}. \quad (7)$$

There are two “ \pm ” and four β . The four β are two pairs according to the \pm in the denominator. We note the denominator is real as the term under the root sign is positive. The existence of the generalized Brillouin zone requires the absolute values of two β in each pair equal to each other. It means the term under the root sign in the numerator is negative, i.e. (see Appendix B for details),

$$(\xi^2 - \Sigma_1 - \Sigma_2)^2 - 4\Sigma_1 \Sigma_2 < 0. \quad (8)$$

Interestingly, the non-Bloch Hamiltonian also gives the same energy spectrum as Eq. (4). It means the topological phase transition also takes place at $\Sigma_1 = \Sigma_2$ in the case with the non-Hermitian skin effect. The open chain is in the topological phase for $\Sigma_1 < \Sigma_2$ and in the trivial phase for $\Sigma_1 > \Sigma_2$. We note the same energy spectrum is a coincidence. The conventional bulk-boundary correspondence still fails as the Bloch spectrum can not provide the open-boundary spectrum.

Figures 2(b) and 2(c) are typical energy spectra of the quadratic system with the emergence of the non-Hermitian skin effect. The energy spectra is all real when $|t_1/\Delta_1| > 1$, although the Bloch spectrum can be complex. We observe a topological phase transition at $t_1 = 1 = \sqrt{|t_2|^2 - |\Delta_2|^2 + |\Delta_1|^2}$, as predicted by the non-Bloch theory.

III. COVARIANCE APPROACH BASED ON QUANTUM MASTER EQUATIONS

We focus on the stationary quantum behaviors of the system, which can be obtained by calculating the time evolution of the system and taking the long-time limits or directly calculating the time-independent equilibrium solutions. In this section, we use the covariance approach based on quantum master equations to obtain exact numerical results.

The quantum master equation is given by $\dot{\rho} = i[\rho, H] + \kappa(1 + n_{\text{th}}) \sum_{j=1}^{2N} \mathcal{D}(a_j)\rho + \kappa n_{\text{th}} \sum_{j=1}^{2N} \mathcal{D}(a_j^\dagger)\rho$, where $\mathcal{D}(\hat{o})\rho = \hat{o}\rho\hat{o}^\dagger - (\hat{o}^\dagger\hat{o}\rho + \rho\hat{o}^\dagger\hat{o})/2$ is the Liouvillian for operator \hat{o} , and n_{th} is the environment photon number.

This equation gives all the information of the density matrix, but the Hilbert space of bosonic systems is infinity, so the truncation process is required, and it still consumes too much computational resources.

To capture the most important features of quantum correlations, we only need to consider the covariances (second-order moments) $\langle \hat{o}\hat{o}' \rangle$, where $\hat{o}, \hat{o}' \in \{a_j, a_j^\dagger, j = 1, 2, \dots, N\}$ are either an annihilation or creation operator. By using this covariance approach we can obtain exact numerical results without truncation process [56]. The evolution equations of the second-order moments can be obtained from the quantum master equations $d\langle \hat{o}\hat{o}' \rangle/dt = \text{Tr}(\dot{\rho}\hat{o}\hat{o}')$, which allow us to numerically analyze both the dynamic and stationary behaviors of the system. To obtain the stationary mean values of the second-order moments, we can let the time derivations equal to zero. Specifically, we are interested in the entanglement between two edge modes a_1 and a_{2N} . Then the degree of the two-mode entanglement can be quantified by the logarithmic negativity E_N , which is a function of the covariance matrix of the two modes [37,57].

IV. ANALYTICAL RESULTS THROUGH QUANTUM LANGEVIN EQUATIONS

Although the exact numerical results can be obtained using the approach in the previous section, the underlying physical mechanism is hard to analyze. In this section we calculate the quantum Langevin equations which provide an approximate route to capture the physical mechanism analytically.

From the original system Hamiltonian in Eq. (1), we can find that the Langevin equations of a quadratic system include both the annihilation and creation operators, which is difficult to be solved analytically. To overcome this problem, we employ a squeezing transformation to transform the quadratic Hamiltonian into a Hamiltonian without the quadratic interactions [47], and the squeezing property now is transformed to the noise operators. For simplicity in calculation, we first rewrite the system Hamiltonian in the quadrature representation [$a_j = (x_j + ip_j)/\sqrt{2}$], which is

$$\begin{aligned} H = & \sum_{j=1}^N [(t_1 + \Delta_1)x_{2j-1}x_{2j} + (t_1 - \Delta_1)p_{2j-1}p_{2j}] \\ & + \sum_{j=1}^{N-1} [(t_2 + \Delta_2)x_{2j+1}x_{2j} + (t_2 - \Delta_2)p_{2j+1}p_{2j}]. \end{aligned} \quad (9)$$

We employ the squeezing transformation $x_j = e^{-r_j}\tilde{x}_j$ and $p_j = e^{r_j}\tilde{p}_j$, then the quadratic Hamiltonian becomes the Hamiltonian of a simple SSH chain

$$\begin{aligned} \tilde{H} = & \sum_{j=1}^N t'_1(\tilde{x}_{2j-1}\tilde{x}_{2j} + \tilde{p}_{2j-1}\tilde{p}_{2j}) \\ & + \sum_{j=1}^{N-1} t'_2(\tilde{x}_{2j}\tilde{x}_{2j+1} + \tilde{p}_{2j}\tilde{p}_{2j+1}) \\ = & \sum_{j=1}^N t'_1 \tilde{a}_{2j-1}^\dagger \tilde{a}_{2j} + \sum_{j=1}^{N-1} t'_2 \tilde{a}_{2j+1}^\dagger \tilde{a}_{2j} + \text{H.c.}, \end{aligned} \quad (10)$$

where $t'_j = \sqrt{t_j^2 - \Delta_j^2}$ for $j = 1, 2$. The site-dependent squeezing parameters in the squeezing transformation are given by

$$r_{2j-1} = (j-1)(r_b - r_a) + r_0, \quad (11)$$

$$r_{2j} = -j(r_b - r_a) + r_b - r_0, \quad (12)$$

where $e^{2r_a} = (t_1 + \Delta_1)/(t_1 - \Delta_1)$ and $e^{2r_b} = (t_2 + \Delta_2)/(t_2 - \Delta_2)$. r_0 is a constant that can be arbitrarily chosen in the squeezing transformation. Here we determine it through the mirror symmetry, i.e., $r_1 = r_{2N}$, which can simplify the calculation of the Langevin equations.

Then we can obtain the Langevin equations of the new operators as

$$\dot{\tilde{a}}_{2j-1} = -\frac{\kappa}{2}\tilde{a}_{2j-1} - it'_1\tilde{a}_{2j} - it'_2\tilde{a}_{2j-2} - \sqrt{\kappa}\tilde{a}_{\text{in},2j-1}, \quad (13)$$

$$\dot{\tilde{a}}_{2j} = -\frac{\kappa}{2}\tilde{a}_{2j} - it'_1\tilde{a}_{2j-1} - it'_2\tilde{a}_{2j+1} - \sqrt{\kappa}\tilde{a}_{\text{in},2j}, \quad (14)$$

where $\tilde{a}_{\text{in},j}$ are the noise operators. Due to the squeezing transformation, these noise operators denote couplings to a squeezed environment. The above Langevin equations can be rewritten in the matrix form as

$$\dot{\tilde{\mathbf{A}}} = \left(-\frac{\kappa}{2}\mathbb{1} - iS\right)\tilde{\mathbf{A}} - \sqrt{\kappa}\tilde{\mathbf{A}}_{\text{in}}, \quad (15)$$

where $\tilde{\mathbf{A}} = (\tilde{a}_1, \dots)^T$, $\tilde{\mathbf{A}}_{\text{in}} = (\tilde{a}_{1,\text{in}}, \dots)^T$, $\mathbb{1}$ is the identity matrix, and S is the coupling matrix (see Appendix C for details). Importantly, after the squeezing transformation, the coupling matrix S is Hermitian and can be diagonalized as $S = PJP^{-1}$. $P = (\boldsymbol{\alpha}_1, \boldsymbol{\alpha}_2, \dots)$ and the column vectors $\boldsymbol{\alpha}_j$ are the eigenvectors of S . The diagonal elements of the diagonal matrix $J = \text{Diag}(\lambda_1, \lambda_2, \dots)$ are the corresponding eigenvalues. Then we can obtain the stationary solutions as

$$\tilde{\mathbf{A}}_s = \sqrt{\kappa} \sum_{j=1}^{2N} \lim_{t \rightarrow \infty} \int_0^t e^{(-\frac{\kappa}{2} - i\lambda_j)(t-t')} [\boldsymbol{\alpha}_j \cdot \tilde{\mathbf{A}}_{\text{in}}(t')] \boldsymbol{\alpha}_j dt' \quad (16)$$

or

$$\tilde{a}_{m,s} = \sqrt{\kappa} \sum_{j,k} \lim_{t \rightarrow \infty} \int_0^t e^{(-\frac{\kappa}{2} - i\lambda_j)(t-t')} \alpha_{j,k} \alpha_{j,m} \tilde{a}_{\text{in},k}(t') dt'. \quad (17)$$

Following the stationary solutions, the mean values of the second-order moments can be obtained as

$$\langle \tilde{a}_m^\dagger \tilde{a}_{m'} \rangle_s = \sum_{j,k,j'} \frac{\kappa \alpha_{j,k} \alpha_{j,m} \alpha_{j',k} \alpha_{j',m'}}{\kappa + i(-\lambda_j^* + \lambda_{j'})} \frac{e^{2r_k} + e^{-2r_k} - 2}{4}, \quad (18)$$

$$\langle \tilde{a}_m \tilde{a}_{m'} \rangle_s = \sum_{j,k,j'} \frac{\kappa \alpha_{j,k} \alpha_{j,m} \alpha_{j',k} \alpha_{j',m'}}{\kappa + i(\lambda_j + \lambda_{j'})} \frac{e^{2r_k} - e^{-2r_k}}{4}. \quad (19)$$

Here and below the summation range is from 1 to $2N$ if there is no additional description. For simplicity, we have assumed the environment photon number $n_{\text{th}} = 0$, and the full expressions can be found in Appendix C.

V. HINT FROM THE TWO-MODE SYSTEM

In this section we analyze the quantum behaviors of a two-mode system, which is a special case of $N = 1$ and can

be solved analytically without approximation, so that we can obtain some hints on the quantum entanglement generation. Following the derivation in Sec. IV, for two-mode system the squeezing parameters are $r_1 = r_2 = r_0 = r_a/2$. The eigenvalues and the eigenvectors are $\lambda_1 = -\lambda_2 = t'_1$ and $\boldsymbol{\alpha}_1 = (1/\sqrt{2}, 1/\sqrt{2})^T$, $\boldsymbol{\alpha}_2 = (1/\sqrt{2}, -1/\sqrt{2})^T$. So the mean values of the second-order moments are

$$\langle \tilde{a}_1^\dagger \tilde{a}_1 \rangle_s = \langle \tilde{a}_2^\dagger \tilde{a}_2 \rangle_s = \frac{e^{r_a} + e^{-r_a} - 2}{4}, \quad (20)$$

$$\langle \tilde{a}_1^\dagger \tilde{a}_2 \rangle_s = 0, \quad (21)$$

$$\langle \tilde{a}_1^2 \rangle_s = \langle \tilde{a}_2^2 \rangle_s = \frac{\kappa^2}{\kappa^2 + 4t_1'^2} \frac{e^{r_a} - e^{-r_a}}{4}, \quad (22)$$

$$\langle \tilde{a}_1 \tilde{a}_2 \rangle_s = -\frac{2i\kappa t_1'}{\kappa^2 + 4t_1'^2} \frac{e^{r_a} - e^{-r_a}}{4}. \quad (23)$$

From the squeezing correlation term (23) we can find that the quantum correlation depends on two factors. The first factor is the squeezing parameter r_a . The squeezing correlation term becomes zero when $r_a = 0$, i.e., $\Delta_1 = 0$, which reveals that the existing of squeezing interaction is necessary for the emergence of stationary correlations. The second factor is the ratio between the dissipation rate κ and the effective coupling strength t'_1 . According to the fluctuation-dissipation theorem, the dissipation of a system is always connected to the noise fluctuation from the environment, so both processes correspond to the same parameter κ denoting system-environment coupling, which appears both at the denominator and numerator in Eq. (23). When $\kappa \ll t'_1$, the squeezing correlation will be suppressed because the coupling to the environment fluctuation is weak. On the other hand, when $\kappa \gg t'_1$, the strong dissipation will also suppress the squeezing correlation. Therefore, the optimal squeezing correlation is obtained for a moderate κ/t'_1 , which means that the system-environment coupling should match the intrasystem coupling. From Eq. (23) we can find that the optimal condition is $\kappa = 2t'_1$.

The above analysis for the two-mode system provides the physical insights for a bosonic chain with more modes. In this case the energy levels become energy bands, thus, it is natural to consider the effect of eigenenergies. We can infer that the eigenenergies should match the system-environment coupling to obtain optimal squeezing correlation. In the topological phase, there exist topological edge states whose eigenenergies are near zero and separated from the bulk energy bands, thus it offers the opportunity to generate long-range entanglement between two edge modes when the corresponding eigenenergies match the system-environment coupling with near zero κ , while at the same time the squeezing correlations between bulk states are suppressed.

VI. QUANTUM BEHAVIORS IN THE TRIVIAL PHASE

In this section, we will prove that the squeezing correlations in a bosonic quadratic chain with trivial phase are greatly suppressed for small κ (compared to the coupling strength), and there are no stationary entanglements in this case. In the trivial phase for $\Sigma_1 > \Sigma_2$, the lattice spectrum opens a trivial gap, and all the eigenvalues have finite absolute values

which we assume are much larger than the dissipation rate $|\lambda_j| \gg \kappa$. So in the summations (18) and (19), those terms with eigenvalues that cancel out with each other are much larger than other terms. Appropriately, we only consider these large terms, and the summations become

$$\langle \tilde{a}_m^\dagger \tilde{a}_{m'} \rangle_s \approx \sum_{k,j} \alpha_{j,k}^2 \alpha_{j,m} \alpha_{j,m'} \frac{e^{2r_k} + e^{-2r_k} - 2}{4}, \quad (24)$$

$$\langle \tilde{a}_m \tilde{a}_{m'} \rangle_s \approx \sum_{k,j} \alpha_{j,k} \alpha_{j,m} \alpha'_{j,k} \alpha'_{j,m'} \frac{e^{2r_k} - e^{-2r_k}}{4}, \quad (25)$$

where $\alpha'_{j,k}$ denotes the eigenvector with an opposite eigenvalue of $\alpha_{j,k}$. As this system preserves chiral symmetry, the pair of eigenvectors with opposite eigenvalues satisfy $\alpha_{j,2k-1} = \alpha'_{j,2k-1}$, $\alpha_{j,2k} = -\alpha'_{j,2k}$. Moreover, the system preserves mirror symmetry $|\alpha_{j,k}| = |\alpha_{j,2N+1-k}|$. In the meanwhile, the squeezing parameters satisfy $r_k = r_{2N+1-k}$. Consequently, every term in the summation (25) is zero. For a similar reason, the summations in Eq. (18) are equal to zero when m and m' are not both odd or even, as every pair of terms with opposite eigenvalues cancel out ($\alpha_{j,k}^2 \alpha_{j,m} \alpha_{j,m'} + \alpha_{j,k}'^2 \alpha'_{j,m} \alpha'_{j,m'} = 0$). It means the only nonzero terms are those like $\langle \tilde{a}_{2m}^\dagger \tilde{a}_{2m'} \rangle_s$ and $\langle \tilde{a}_{2m+1}^\dagger \tilde{a}_{2m'+1} \rangle_s$.

These properties mean the total lattice can be divided into two sublattices: the odd modes and the even modes. The modes between two sublattices have no quantum correlation. Moreover, as the squeezing correlation terms ($m \neq m'$) or single-mode squeezing terms ($m = m'$) in Eq. (25) are always zero, there is no quantum squeezing effect in the squeezing representation. In other words, the squeezing parameters r_j in the squeezing transformation are exactly the squeezing coefficient of every mode in the steady state.

VII. QUANTUM BEHAVIORS IN THE TOPOLOGICAL PHASE

In the topological phase for $\Sigma_1 < \Sigma_2$, the energy spectrum is different from that in the trivial phase, with the emergence of topological edge states. The absolute energy of two edge states $|\lambda_{1,2}|$ is much smaller than the absolute values of other eigenvalues. Consequently, the contribution of the topological edge states must be considered in the summations. For simplicity, we note that in this work the concept of ‘‘state’’ denotes the eigenstates of the chain, while the concept of ‘‘mode’’ denotes the original physical modes in the chain. The summations of Eqs. (18) and (19) become

$$\begin{aligned} \langle \tilde{a}_m^\dagger \tilde{a}_{m'} \rangle_s &\approx \sum_{k,j} \alpha_{j,k}^2 \alpha_{j,m} \alpha_{j,m'} \frac{e^{2r_k} + e^{-2r_k} - 2}{4} \\ &+ \sum_{k,j=1,2} \frac{\kappa}{\kappa + 2i\lambda_j} \alpha_{j,k} \alpha_{j,m} \alpha'_{j,k} \alpha'_{j,m'} \frac{e^{2r_k} + e^{-2r_k} - 2}{4}, \end{aligned} \quad (26)$$

$$\begin{aligned} \langle \tilde{a}_m \tilde{a}_{m'} \rangle_s &\approx \sum_{k,j} \alpha_{j,k} \alpha_{j,m} \alpha'_{j,k} \alpha'_{j,m'} \frac{e^{2r_k} - e^{-2r_k}}{4} \\ &+ \sum_{k,j=1,2} \frac{\kappa}{\kappa + 2i\lambda_j} \alpha_{j,k}^2 \alpha_{j,m} \alpha_{j,m'} \frac{e^{2r_k} - e^{-2r_k}}{4}. \end{aligned} \quad (27)$$

As proved in the previous section, the first line in Eq. (27) is zero. Similarly, the second line in Eq. (26) is also zero. Then the summation Eq. (26) returns to Eq. (24), but the squeezing correlation terms or single-mode squeezing terms (27) keep nonzero as

$$\langle \tilde{a}_m \tilde{a}_{m'} \rangle_s \approx \sum_{k,j=1,2} \frac{\kappa}{\kappa + 2i\lambda_j} \alpha_{j,k}^2 \alpha_{j,m} \alpha_{j,m'} \frac{e^{2r_k} - e^{-2r_k}}{4}. \quad (28)$$

We point out that Eq. (28) summarizes the key analytical results of this work. The nonzero squeezing correlation terms in Eq. (28) lead to the emergence of two-mode entanglement in the steady state, and the single-mode squeezing terms in Eq. (28) lead to a modulation of squeezing degree and squeezing phase in every mode. Importantly, unlike the terms in Eq. (24) which are non-zero only when m and m' are both odd or even, the terms in Eq. (28) are always nonzero irrespective of m and m' . It denotes that there are also quantum correlations between modes in two sublattices, which do not exist in the trivial phase. Moreover, as shown in the derivation, the nonzero terms in Eq. (28) originate from the near-zero energies of two topological edge modes. So the quantum effects such as the quantum entanglements can be viewed as the quantum signatures of the topological edge modes.

We assume the eigenvalues of two edge states are $\lambda_1 = \delta$ and $\lambda_2 = -\delta$. The distributions of two edge states can be approximately given by $\alpha_{1,2j-1} = \alpha_{2,2j-1} \approx l e^{-(j-1)\varepsilon}$ and $\alpha_{1,2j} = -\alpha_{2,2j} \approx l e^{(j-N)\varepsilon}$, where $\varepsilon \approx \ln t'_2 - \ln t'_1$ is the topological localization coefficient, and $l = 1/\sqrt{2(1 - e^{-2(N-1)\varepsilon})/(1 - e^{-2\varepsilon})}$ is the normalization coefficient [58]. Then Eq. (28) can be reduced to

$$\langle \tilde{a}_{2m} \tilde{a}_{2m'} \rangle_s \approx \frac{\kappa^2 l^4 e^{(m+m'-2N)\varepsilon}}{\kappa^2 + 4\delta^2} [e^{-2r_0} L_1 - e^{2r_0} L_2], \quad (29)$$

$$\langle \tilde{a}_{2m+1} \tilde{a}_{2m'+1} \rangle_s \approx \frac{\kappa^2 l^4 e^{-(m+m'-2)\varepsilon}}{\kappa^2 + 4\delta^2} [e^{-2r_0} L_1 - e^{2r_0} L_2], \quad (30)$$

$$\begin{aligned} \langle \tilde{a}_{2m} \tilde{a}_{2m'+1} \rangle_s \\ \approx -\frac{2i\delta\kappa l^4 e^{(m-m'-N+1)\varepsilon}}{\kappa^2 + 4\delta^2} [e^{-2r_0} L_1 - e^{2r_0} L_2], \end{aligned} \quad (31)$$

where $L_1 = [1 - e^{-2(N-1)(\varepsilon+r_b-r_a)}]/[1 - e^{-2(\varepsilon+r_b-r_a)}]$ and $L_2 = [1 - e^{-2(N-1)(\varepsilon-r_b+r_a)}]/[1 - e^{-2(\varepsilon-r_b+r_a)}]$.

All the above squeezing terms are modulated by the exponential distribution of the topological edge state, and these terms decrease quickly when considering modes far away from the edges. In Fig. 3, we plot the stationary entanglement (quantified by E_N) between two edge modes (red) and between the first mode and the third mode (blue) versus the ratio of linear coupling strengths t_2/t_1 . The maximal stationary entanglement in the latter case is much smaller than in the former case. Moreover, we find that there is no stationary entanglement between other pairs of modes [except between the $(2N-2)$ th and $2N$ th modes].

Therefore, as the absolute eigenenergies of the topological edge states are much smaller than those of the bulk states, we can selectively enhance the stationary entanglement between two topological edge states, when the dissipation rate κ is much smaller than the coupling strengths.

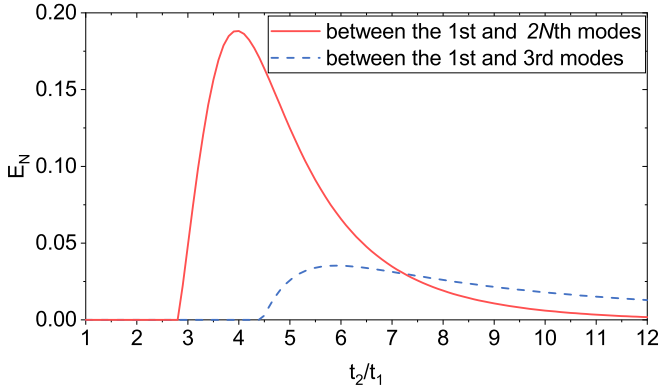


FIG. 3. Stationary entanglement (quantified by E_N) between two edge modes (red solid line) and between the first mode and the third mode (blue dashed line) versus the ratio of linear coupling strengths t_2/t_1 . Other parameters are $\kappa = 0.01$, $N = 5$, $\mu = 0$, and $\Delta_1/t_1 = \Delta_2/t_2 = 0.6$.

VIII. TOPOLOGY-INDUCED ENTANGLEMENT BETWEEN TWO EDGE MODES

As the topological edge states are most distributed at two edge modes, they have the maximal quantum entanglement. For $m, m' \in \{1, N\}$, Eqs. (29)–(31) can be reduced to

$$\langle \tilde{a}_1^2 \rangle_s = \langle \tilde{a}_{2N}^2 \rangle_s \approx \frac{\kappa^2 l^4}{\kappa^2 + 4\delta^2} [e^{-2r_0} L_1 - e^{2r_0} L_2], \quad (32)$$

$$\langle \tilde{a}_1 \tilde{a}_{2N} \rangle_s \approx -\frac{2i\delta\kappa l^4}{\kappa^2 + 4\delta^2} [e^{-2r_0} L_1 - e^{2r_0} L_2]. \quad (33)$$

Moreover, in this case, we can neglect other terms except for $j = 1, 2$ in Eq. (24) because the topological edge states have distinct profiles compared with the bulk states. For $m, m' \in \{1, N\}$, the distributions of the bulk states in Eq. (24) are much smaller than the edge states ($|\alpha_{j,m} \alpha_{j,m'}|_{j=1,2} \gg |\alpha_{j,m} \alpha_{j,m'}|_{j \neq 1,2}$). Consequently, the summations can be reduced to $\langle \tilde{a}_1^\dagger \tilde{a}_{2N} \rangle_s = \langle \tilde{a}_{2N}^\dagger \tilde{a}_1 \rangle_s = 0$ and

$$\langle \tilde{a}_1^\dagger \tilde{a}_1 \rangle_s = \langle \tilde{a}_{2N}^\dagger \tilde{a}_{2N} \rangle_s \approx l^4 (e^{-2r_0} L_1 + e^{2r_0} L_2) - l^2. \quad (34)$$

Due to the symmetry between two edge modes, the logarithmic negativity is given by $E_N = \max[0, -\ln 2\eta^-]$, where $\eta^- = |\sqrt{(1/2 + K_1)^2 - K_2^2 - K_3}|$, and $K_1 = \langle \tilde{a}_{1(2N)}^\dagger \tilde{a}_{1(2N)} \rangle_s$, $K_2 = \langle \tilde{a}_{1(2N)}^2 \rangle_s$, $K_3 = -i \langle \tilde{a}_1 \tilde{a}_{2N} \rangle_s$ are three different stationary mean values of the second-order moments. We note here we directly calculate the logarithmic negativity using the squeezed operators because the value of logarithmic negativity is independent of the squeezing transformation.

To verify the above results, in Figs. 4 and 5 we plot the logarithmic negativity as functions of the system parameters for an open chain with 10 modes ($N = 5$), where both exact numerical results and approximate analytical results are presented. In Fig. 4, the coupling strengths satisfy $t_2/t_1 = 4$, and thus the system is in the topological phase when $|\Delta_2/t_2| < \sqrt{3 + (\Delta_1/t_1)^2}/2$. The green solid line indicates the phase boundary between the topological phase (above the line) and the trivial phase (below the line). In Fig. 5, the coupling strengths satisfy $\Delta_1/t_1 = \Delta_2/t_2$, and thus the system is in the topological phase when $t_2/t_1 > 1$ (including all the regions in

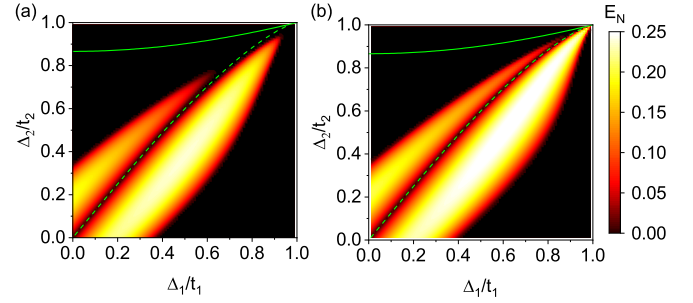


FIG. 4. Stationary entanglement as quantified by the logarithmic negativity E_N between two edge modes as functions of Δ_1/t_1 and Δ_2/t_2 . (a) Exact numerical results obtained from the quantum master equations. (b) Approximate analytical results obtained from the quantum Langevin equations. The green solid line indicates the phase boundary between the trivial phase (above the line) and the topological phase (below the line). The green dashed line indicates the vanished entanglement for $e^{-2r_0} L_1 = e^{2r_0} L_2$. The parameters are $t_2/t_1 = 4$, $N = 5$, and $\kappa = 0.01$.

Fig. 5). We can find that for a wide parameter region in the topological phase, the logarithmic negativity is nonzero.

Remarkably, the approximate analytical results agree well with the exact numerical results obtained from the quantum master equations, which means that our approximations in the derivation of the analytical results perfectly catch the key point of the entanglement phenomenon. It is the existence of the topological edge states that leads to the stationary entanglement between two edge modes.

IX. MAXIMIZING ENTANGLEMENT

The analytical solutions can also help us to understand the pattern of the logarithmic negativity and to maximize the entanglement. In Fig. 4, the logarithmic negativity splits into two bright areas. In the analytical expression, the dark area between the two bright areas corresponds to the case when $e^{-2r_0} L_1 - e^{2r_0} L_2 \approx 0$ (denoted by the green dashed line). The factor $e^{-2r_0} L_1 - e^{2r_0} L_2$ appears both in the squeezing term [cf. Eq. (32)] and in the correlation term [cf. Eq. (33)]. So when the entanglement disappears in the central dark area, the

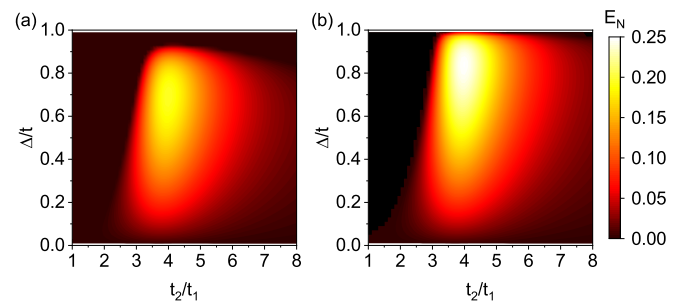


FIG. 5. Stationary entanglement as quantified by the logarithmic negativity E_N between two edge modes as functions of t_2/t_1 and Δ/t for $\Delta_1/t_1 = \Delta_2/t_2$. (a) Exact numerical results obtained from the quantum master equations. (b) Approximate analytical results obtained from the quantum Langevin equations. Other parameters are $N = 5$ and $\kappa = 0.01$.

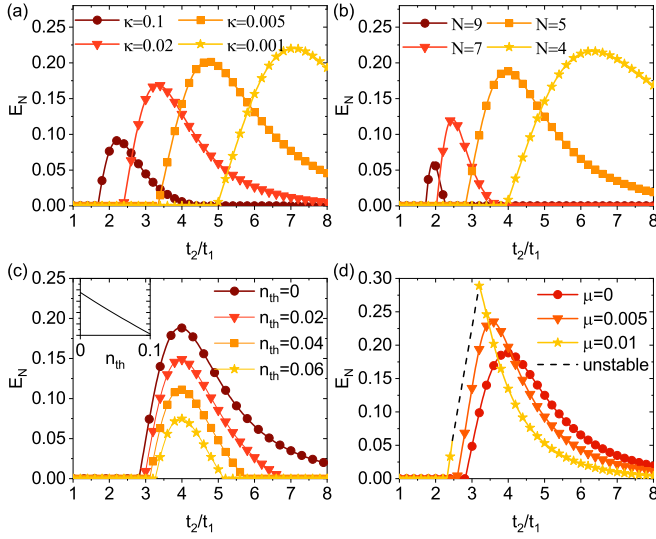


FIG. 6. Stationary entanglement between two edge modes (quantified by E_N) versus the ratio of linear coupling strengths t_2/t_1 considering the influence of the dissipation rate κ (a), the number of the unit cell N (b), the environment photon number n_{th} (c), and the chemical potential μ (d). The squeezing interactions satisfy $\Delta_1/t_1 = \Delta_2/t_2 = 0.6$. The inset of (c) is the logarithmic negativity E_N as a function of n_{th} for $t_2/t_1 = 4$. The dashed line in (d) denotes the region where the system is unstable (no stationary solutions). Other parameters are $\mu = 0$ in (a), (b), and (c); $N = 5$ in (a), (c), and (d); $n_{\text{th}} = 0$ in (a), (b), and (d); $\kappa = 0.01$ in (b), (c), and (d).

steady state of every mode is nearly an unsqueezed coherent state in the squeezing representation (but a squeezed state in the original representation), which is similar to the behaviors in the trivial phase. In this case, the entanglement is totally suppressed and there is only the single-mode squeezing effect.

We then focus on the special case $\Delta_1/t_1 = \Delta_2/t_2$ considered in Fig. 5. It is the condition when the non-Hermitian skin effect disappears ($\Sigma_1 \Sigma_2 = \Sigma_3^2$). In this case, the squeezing parameters become $r_a = r_b = 2r_0$, and the mean values of the second-order moments [cf. Eqs. (32)–(34)] can be greatly reduced, which are

$$\langle \tilde{a}_1^\dagger \tilde{a}_1 \rangle_s = \langle \tilde{a}_{2N}^\dagger \tilde{a}_{2N} \rangle_s \approx l^2 \frac{e^{-2r_0} + e^{2r_0} - 2}{2}, \quad (35)$$

$$\langle \tilde{a}_1^2 \rangle_s = \langle \tilde{a}_{2N}^2 \rangle_s \approx \frac{\kappa^2 l^2}{\kappa^2 + 4\delta^2} \frac{e^{-2r_0} - e^{2r_0}}{2}, \quad (36)$$

$$\langle \tilde{a}_1 \tilde{a}_{2N} \rangle_s \approx -\frac{2i\delta\kappa l^2}{\kappa^2 + 4\delta^2} \frac{e^{-2r_0} - e^{2r_0}}{2}. \quad (37)$$

Then the logarithmic negativity mainly depends on the interplay between the dissipation κ and the absolute energy of the topological edge modes δ . According to Eqs. (36) and (37), the maximal logarithmic negativity is obtained near $\kappa = 2\delta$. We note that the absolute energy of the topological edge modes δ is smaller when the ratio t_2/t_1 is larger. Inversely, the absolute energy δ is smaller when the number of unit cells N is smaller. So for a smaller dissipation rate or a smaller unit-cell number, the maximal entanglement is obtained at a larger ratio t_2/t_1 , as shown in Figs. 6(a) and 6(b).

We also investigate the influence of the environment photon number n_{th} and the chemical potential (onsite energy)

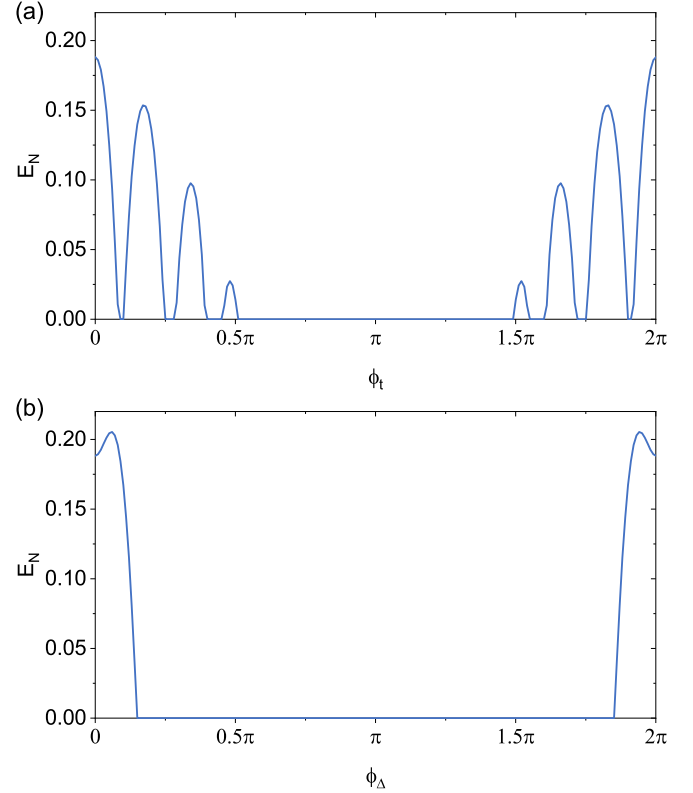


FIG. 7. Stationary entanglement (quantified by E_N) between two edge modes versus the coupling phase ϕ_t (a) and ϕ_Δ (b). Other parameters are $\kappa = 0.01$, $N = 5$, $\mu = 0$, $t_1 = 1$, $|t_2| = 4$, and $\Delta_1/t_1 = |\Delta_2/t_2| = 0.6$.

μ on the stationary entanglement, which are not included in the above calculation. For simplicity, we assume n_{th} and μ of all modes are the same. As plotted in Fig. 6(c), the stationary entanglement decays linearly when increasing the environment photon number n_{th} . As shown in Fig. 6(d), the chemical potential will also affect the entanglement. In some parameter ranges when the system is in the stable region, the chemical potential can enhance the maximal entanglement, while it can also enhance the instability due to the intrinsic non-Hermiticity of the squeezing interactions.

X. STATIONARY ENTANGLEMENTS WITH COMPLEX-VALUED COUPLINGS

As shown in Sec. II, the topological phase transition is independent of the coupling phases. However, the stationary entanglements are highly dependent on the coupling phases. This is because the squeezing transformation is phase dependent. Figure 7 plots the stationary entanglement (quantified by E_N) between two edge modes versus the coupling phase ϕ_t and ϕ_Δ . The stationary entanglement exhibits an interesting fingerlike pattern versus the coupling phase ϕ_t , while there is stationary entanglement only for a small range of coupling phase ϕ_Δ near 0 or 2π .

In particular, the case for π phase can be understood through the analytical expression, as the coupling strengths are still real. The cases for $\phi_t = \pi$ and $\phi_\Delta = \pi$ are equivalent. For example, in the case of $\phi_\Delta = \pi$, the squeezing parameters

r_b in the squeezing transformation become negative, while r_a is still positive. Then the squeezing parameter of every mode r_j is greatly enhanced, which leads to more enhancement of the stationary photon number (34) than the enhancement of the squeezing correlation (32), so the quantum entanglement disappears.

XI. EXPERIMENTAL REALIZATION

The main requirements of the system are site-dependent coupling strengths and the squeezing interactions. These requirements are already satisfied by a recent experiment based on an optomechanical cavity [49]. They make use of the idea of synthetic dimension realized from multiple nondegenerate mechanical modes. These mechanical modes are coupled to an optical cavity mode through the radiation pressure, and the optical cavity mode can be used to generate both the beam-splitter (linear) and squeezing interactions between different mechanical modes. These couplings are obtained through modulation at a special frequency in the large-detuning regime. Moreover, the coupling strengths can be individually controlled by the modulation depth. So the multimode optomechanical system is a perfect platform to realize the topology-induced entanglement, and the stationary entanglement can be read out by an additional probe laser. As shown in Fig. 6(b), there are obvious quantum entanglements for only four modes.

XII. DISCUSSION AND CONCLUSION

We establish a direct relationship between quantum entanglement and classical topology. It is distinct from the proposals utilizing topology to enhance the robustness of quantum effects [59–66]. It is also different from the efforts to include quantum effects to obtain novel topological phase transition [67–69]. Our work shows that the bosonic topology can be a source of the quantum entanglements and the quantum entanglements can be a quantum signature of the topological phase. It also has the potential to investigate quantum phase transition driven by bosonic topology.

The results in this work reveal a general mechanism that can be applied to various systems and can be generalized to higher dimensions. For example, this mechanism can be directly applied to the lattice model with dissipative pairing interactions [52] and the model with single-mode squeezing [67]. Moreover, this mechanism can be generalized to high-dimensional systems such as the higher-order topological corner modes, and the mechanism can also be used to generate quantum entanglements as a witness of the Floquet topology.

We note that the relationship between topology and entanglement is only valid in bosonic quadratic systems, as the quadratic squeezing interactions are the source of entanglement. In no-quadratic systems, there is no squeezing or entanglement, and we can not investigate the relationship between the topology and the entanglement. Moreover, although the bosonic quadratic systems possess non-Hermitian dynamics and may exhibit non-Hermitian skin effects. The relationship between topology and entanglement we find here is irrelevant without the non-Hermitian skin effects.

In summary, we discover that there is a topology-induced entanglement effect in the steady state of a bosonic quadratic chain. We show the stationary entanglement only exists in the topological phase. The relation between the entanglement and the topological edge states is established with analytical expressions by appropriately solving the quantum Langevin equations, where we neglect the terms containing bulk-state eigenenergies but keep the terms containing near-zero eigenenergies which correspond to the topological edge states. The analytical results show good agreement with the numerical results obtained from the covariance approach based on the quantum master equations, which proves that our approximation perfectly catches the key point of the emerging entanglement phenomenon. We verify that the approximation is valid because the squeezing correlations are greatly suppressed when the intrasystem coupling strengths (which determine the system eigenenergies) do not match the system-environment coupling strengths (denoted by the dissipation rate). For a topological system, the topological edge states possess near-zero eigenenergies, which are much smaller than the absolute value of the eigenenergies of the bulk states, so we can selectively match the topological edge states with the system-environment coupling and generate obvious stationary entanglements between these states. This kind of topological matching and related entanglements disappears in the trivial phase when there are no topological edge states. Based on this finding, we thoroughly discuss the influence of different parameters on the stationary entanglements and maximal conditions. This model is implementable in a variety of experimental platforms, such as multimode optomechanical systems and superconducting quantum circuits. Our work opens an avenue for investigating quantum entanglement in topological systems.

ACKNOWLEDGMENTS

This work is supported by the National Key R&D Program of China (Grant No. 2023YFA1407600), and the National Natural Science Foundation of China (NSFC) (Grants No. 12275145, No. 92050110, No. 91736106, No. 11674390, and No. 91836302).

APPENDIX A: BLOCH THEORY FOR A QUADRATIC CHAIN

In this Appendix, we provide a detailed calculation of the Bloch theory for a quadratic chain with staggered couplings. The Hamiltonian is written as

$$H = \sum_{j=1}^N (t_1 a_{2j-1}^\dagger a_{2j} + \Delta_1 a_{2j-1}^\dagger a_{2j}^\dagger + \text{H.c.}) + \sum_{j=1}^{N-1} (t_2 a_{2j+1}^\dagger a_{2j} + \Delta_2 a_{2j+1}^\dagger a_{2j}^\dagger + \text{H.c.}), \quad (\text{A1})$$

where t_1 (t_2) and Δ_1 (Δ_2) are the intracell (intercell) coupling strengths of linear and squeezing interactions, respectively, N is the number of unit cells, and a_j is the annihilation operator of the j th mode. After the Fourier transformation, the Bloch Hamiltonian of the system can be written as

$$\mathcal{H}(k) = (t_1 + t_2 e^{ik})a_k^\dagger a'_k + (\Delta_1 + \Delta_2 e^{ik})a_k^\dagger a'_{-k} + \text{H.c.}, \quad (\text{A2})$$

or in the matrix form $\mathcal{H}(k) = \frac{1}{2}C_k^\dagger \mathcal{H}_M(k)C_k$, where $C_k^\dagger = (a_k^\dagger, a'_k, a_{-k}, a'_{-k})$ and

$$\mathcal{H}_M(k) = \begin{pmatrix} 0 & t_1 + t_2 e^{ik} & 0 & \Delta_1 + \Delta_2 e^{ik} \\ t_1^* + t_2^* e^{-ik} & 0 & \Delta_1 + \Delta_2 e^{-ik} & 0 \\ 0 & \Delta_1^* + \Delta_2^* e^{ik} & 0 & t_1^* + t_2^* e^{ik} \\ \Delta_1^* + \Delta_2^* e^{-ik} & 0 & t_1 + t_2 e^{-ik} & 0 \end{pmatrix}. \quad (\text{A3})$$

Here the excitation modes are Bogoliubov modes that are determined by the eigenvalue equation of $\tau_z \mathcal{H}_M$, where $\tau_z = \text{Diagonal}(\mathbb{1}, -\mathbb{1})$ and $\mathbb{1}$ is an identity matrix with half the dimension of the corresponding Hamiltonian [48]. The eigenvalue equation $\det|\tau_z \mathcal{H}_M - \xi \mathbb{1}| = 0$ can be obtained as

$$(\xi^2 - |t_1 + t_2 e^{ik}|^2)(\xi^2 - |t_1 + t_2 e^{-ik}|^2) + \xi^2(|\Delta_1 + \Delta_2 e^{ik}|^2 + |\Delta_1 + \Delta_2 e^{-ik}|^2) + |(\Delta_1 + \Delta_2 e^{ik})(\Delta_1 + \Delta_2 e^{-ik})|^2 - 2 \text{Re}[(t_1 + t_2 e^{ik})(t_1^* + t_2^* e^{ik})(\Delta_1 + \Delta_2 e^{-ik})(\Delta_1^* + \Delta_2^* e^{-ik})] = 0. \quad (\text{A4})$$

Consequently, only the relative phases between t_1 (Δ_1) and t_2 (Δ_2) are important. So we can assume

$$t_2 = q_t t_1 e^{i\phi_t}, \quad \Delta_2 = q_\Delta \Delta_1 e^{i\phi_\Delta}, \quad (\text{A5})$$

where $q_{t,\Delta}$, t_1 , and Δ_1 are all real, ϕ_t (ϕ_Δ) are the relative phases between t_1 (Δ_1) and t_2 (Δ_2), respectively. So Eq. (A4) can be rewritten as

$$\begin{aligned} & \xi^4 - 2\xi^2[(1 + q_t^2 + 2q_t \cos k \cos \phi_t)t_1^2 - (1 + q_\Delta^2 + 2q_\Delta \cos k \cos \phi_\Delta)\Delta_1^2] \\ & + [1 + q_t^2 + 2q_t \cos(k + \phi_t)][1 + q_t^2 + 2q_t \cos(k - \phi_t)]t_1^4 \\ & + [1 + q_\Delta^2 + 2q_\Delta \cos(k + \phi_\Delta)][1 + q_\Delta^2 + 2q_\Delta \cos(k - \phi_\Delta)]\Delta_1^4 \\ & - 2 \text{Re}[(1 + 2q_t e^{ik} \cos \phi_t + q_t^2 e^{2ik})(1 + 2q_\Delta e^{-ik} \cos \phi_\Delta + q_\Delta^2 e^{-2ik})]t_1^2 \Delta_1^2 = 0. \end{aligned} \quad (\text{A6})$$

Then we can obtain

$$\begin{aligned} \xi^2 &= (1 + q_t^2 + 2q_t \cos k \cos \phi_t)t_1^2 - (1 + q_\Delta^2 + 2q_\Delta \cos k \cos \phi_\Delta)\Delta_1^2 \\ & \pm 2|\sin k| \sqrt{(q_t \sin \phi_t t_1^2)^2 + (q_\Delta \sin \phi_\Delta \Delta_1^2)^2 - t_1^2 \Delta_1^2 (q_t^2 + q_\Delta^2 - 2q_t q_\Delta \cos \phi_t \cos \phi_\Delta)} \end{aligned} \quad (\text{A7})$$

or

$$\begin{aligned} \xi^2 &= (1 + q_t^2 + 2q_t \cos k \cos \phi_t)t_1^2 - (1 + q_\Delta^2 + 2q_\Delta \cos k \cos \phi_\Delta)\Delta_1^2 \\ & \pm 2|\sin k| \sqrt{(q_t^2 t_1^2 - q_\Delta^2 \Delta_1^2)(t_1^2 - \Delta_1^2) - (q_t \cos \phi_t t_1^2 - q_\Delta \cos \phi_\Delta \Delta_1^2)^2}. \end{aligned} \quad (\text{A8})$$

For simplicity, we let $\Sigma_1 = t_1^2 - \Delta_1^2$, $\Sigma_2 = q_t^2 t_1^2 - q_\Delta^2 \Delta_1^2$, and $\Sigma_3 = q_t \cos \phi_t t_1^2 - q_\Delta \cos \phi_\Delta \Delta_1^2$. So Eq. (A8) becomes

$$\xi^2 = \Sigma_1 + \Sigma_2 + 2\Sigma_3 \cos k \pm 2|\sin k| \sqrt{\Sigma_1 \Sigma_2 - \Sigma_3^2}, \quad (\text{A9})$$

corresponding to Eq. (3) in the main text. When $\Sigma_1 \Sigma_2 - \Sigma_3^2 > 0$, the system does not exhibit the non-Hermitian skin effect. In this case, Eq. (A9) can be rewritten as

$$\xi^2 = \Sigma_1 + \Sigma_2 + 2\Sigma_1 \Sigma_2 \cos(\pm k + \varphi), \quad (\text{A10})$$

where $\tan \varphi = \sqrt{\Sigma_1 \Sigma_2 - \Sigma_3^2} / \Sigma_3$. Then we can obtain the energy spectrum as

$$(\sqrt{\Sigma_1} - \sqrt{\Sigma_2})^2 < \xi^2 < (\sqrt{\Sigma_1} + \sqrt{\Sigma_2})^2, \quad (\text{A11})$$

where we assume $\Sigma_{1,2}$ are both positive.

APPENDIX B: NON-BLOCH THEORY FOR A QUADRATIC CHAIN

When there is the non-Hermitian skin effect, i.e., $\Sigma_1 \Sigma_2 - \Sigma_3^2 < 0$, the Bloch theory fails in the calculation of the open-boundary bulk spectrum. Then we need to use the non-Bloch theory, with the replacements $e^{ik} \rightarrow \beta$ and $e^{-ik} \rightarrow \beta^{-1}$. So the

non-Bloch Hamiltonian matrix can be written as

$$\mathcal{H}_M(\beta) = \begin{pmatrix} 0 & t_1 + t_2\beta & 0 & \Delta_1 + \Delta_2\beta \\ t_1^* + t_2^*\beta^{-1} & 0 & \Delta_1 + \Delta_2\beta^{-1} & 0 \\ 0 & \Delta_1^* + \Delta_2^*\beta & 0 & t_1^* + t_2^*\beta \\ \Delta_1^* + \Delta_2^*\beta^{-1} & 0 & t_1 + t_2\beta^{-1} & 0 \end{pmatrix}. \quad (\text{B1})$$

The eigenvalue equation $\det|\tau_z \mathcal{H}_M - \xi \mathbb{1}| = 0$ is

$$\begin{aligned} & \xi^4 - 2\xi^2 \{ [1 + q_t^2 + q_t \cos \phi_t (\beta + \beta^{-1})] t_1^2 - [1 + q_\Delta^2 + q_\Delta \cos \phi_\Delta (\beta + \beta^{-1})] \Delta_1^2 \} \\ & + \{ [1 + q_t^2 + q_t \cos \phi_t (\beta + \beta^{-1})]^2 + [q_t \sin \phi_t (\beta - \beta^{-1})]^2 \} t_1^4 \\ & + \{ [1 + q_\Delta^2 + q_\Delta \cos \phi_\Delta (\beta + \beta^{-1})]^2 + [q_\Delta \sin \phi_\Delta (\beta - \beta^{-1})]^2 \} \Delta_1^4 \\ & - [2(1 + q_t^2 q_\Delta^2) + (q_t^2 + q_\Delta^2)(\beta^2 + \beta^{-2}) + 8 \cos \phi_t \cos \phi_\Delta q_t q_\Delta] t_1^2 \Delta_1^2 \\ & - 2[\cos \phi_t q_t (1 + q_\Delta^2) + \cos \phi_\Delta q_\Delta (1 + q_t^2)] (\beta + \beta^{-1}) t_1^2 \Delta_1^2 = 0. \end{aligned} \quad (\text{B2})$$

Then we obtain

$$\begin{aligned} \xi^2 &= [1 + q_t^2 + q_t \cos \phi_t (\beta + \beta^{-1})] t_1^2 - [1 + q_\Delta^2 + q_\Delta \cos \phi_\Delta (\beta + \beta^{-1})] \Delta_1^2 \\ &\pm \sqrt{-(\beta - \beta^{-1})^2 \sqrt{(q_t \sin \phi_t t_1^2)^2 + (q_\Delta \sin \phi_\Delta \Delta_1^2)^2} - t_1^2 \Delta_1^2 (q_t^2 + q_\Delta^2 - 2q_t q_\Delta \cos \phi_t \cos \phi_\Delta)}, \end{aligned} \quad (\text{B3})$$

or

$$\begin{aligned} \xi^2 &= [1 + q_t^2 + q_t \cos \phi_t (\beta + \beta^{-1})] t_1^2 - [1 + q_\Delta^2 + q_\Delta \cos \phi_\Delta (\beta + \beta^{-1})] \Delta_1^2 \\ &\pm \sqrt{-(\beta - \beta^{-1})^2 \sqrt{(q_t^2 t_1^2 - q_\Delta^2 \Delta_1^2) (t_1^2 - \Delta_1^2)} - (q_t \cos \phi_t t_1^2 - q_\Delta \cos \phi_\Delta \Delta_1^2)^2}. \end{aligned} \quad (\text{B4})$$

We can also obtain the generalized momentum as

$$\beta = \frac{1}{2} \frac{\lambda^2 - (1 + q_t^2) t_1^2 + (1 + q_\Delta^2) \Delta_1^2 \pm \sqrt{[\xi^2 - (1 + q_t^2) t_1^2 + (1 + q_\Delta^2) \Delta_1^2]^2 - 4(q_t^2 t_1^2 - q_\Delta^2 \Delta_1^2) (t_1^2 - \Delta_1^2)}}{q_t \cos \phi_t t_1^2 - q_\Delta \cos \phi_\Delta \Delta_1^2 \pm \sqrt{(q_t \cos \phi_t t_1^2 - q_\Delta \cos \phi_\Delta \Delta_1^2)^2 - (q_t^2 t_1^2 - q_\Delta^2 \Delta_1^2) (t_1^2 - \Delta_1^2)}}. \quad (\text{B5})$$

There are two “ \pm ” and four β . The four β are two pairs according to the \pm in the denominator. We note the denominator is real as the term under the root sign is positive. The existence of the generalized Brillouin zone requires the absolute values of two β in each pair equal to each other. To be clear, we let

$$\beta_{i,\pm} = \frac{1}{2} \frac{\lambda^2 - (1 + q_t^2) t_1^2 + (1 + q_\Delta^2) \Delta_1^2 \pm \sqrt{[\xi^2 - (1 + q_t^2) t_1^2 + (1 + q_\Delta^2) \Delta_1^2]^2 - 4(q_t^2 t_1^2 - q_\Delta^2 \Delta_1^2) (t_1^2 - \Delta_1^2)}}{q_t \cos \phi_t t_1^2 - q_\Delta \cos \phi_\Delta \Delta_1^2 + (-1)^i \sqrt{(q_t \cos \phi_t t_1^2 - q_\Delta \cos \phi_\Delta \Delta_1^2)^2 - (q_t^2 t_1^2 - q_\Delta^2 \Delta_1^2) (t_1^2 - \Delta_1^2)}}, \quad (\text{B6})$$

for $i = 1, 2$. The requirement becomes $|\beta_{i,+}| = |\beta_{i,-}|$, which means the term under the root sign in the numerator is negative, i.e.,

$$[\xi^2 - (1 + q_t^2) t_1^2 + (1 + q_\Delta^2) \Delta_1^2]^2 - 4(q_t^2 t_1^2 - q_\Delta^2 \Delta_1^2) (t_1^2 - \Delta_1^2) < 0. \quad (\text{B7})$$

So we can obtain the energy spectrum as

$$(\sqrt{t_1^2 - \Delta_1^2} - \sqrt{q_t^2 t_1^2 - q_\Delta^2 \Delta_1^2})^2 < \lambda^2 < (\sqrt{t_1^2 - \Delta_1^2} + \sqrt{q_t^2 t_1^2 - q_\Delta^2 \Delta_1^2})^2, \quad (\text{B8})$$

which is the same as the energy spectrum (4) for $\Sigma_1 \Sigma_2 - \Sigma_3^2 > 0$ when there is no non-Hermitian skin effect.

APPENDIX C: DERIVATION OF THE QUANTUM LANGEVIN EQUATIONS

We start from the quantum Langevin equations of operators after the squeezing transformation [Eqs. (13) and (14)], which are

$$\dot{\tilde{a}}_{2j-1} = -\frac{\kappa}{2} \tilde{a}_{2j-1} - it'_1 \tilde{a}_{2j} - it'_2 \tilde{a}_{2j-2} - \sqrt{\kappa} \tilde{a}_{\text{in},2j-1}, \quad (\text{C1})$$

$$\dot{\tilde{a}}_{2j} = -\frac{\kappa}{2} \tilde{a}_{2j} - it'_1 \tilde{a}_{2j-1} - it'_2 \tilde{a}_{2j+1} - \sqrt{\kappa} \tilde{a}_{\text{in},2j}, \quad (\text{C2})$$

where $\tilde{a}_{in,j}$ are the noise operators. Due to the squeezing transformation, these noise operators denote couplings to a squeezed environment. The above Langevin equations can be rewritten in the matrix form as

$$\dot{\tilde{\mathbf{A}}} = \left(-\frac{\kappa}{2}\mathbb{1} - iS\right)\tilde{\mathbf{A}} - \sqrt{\kappa}\tilde{\mathbf{A}}_{in}, \quad (\text{C3})$$

where $\mathbb{1}$ is the identity matrix, $\tilde{\mathbf{A}} = (\tilde{a}_1, \dots)^T$, $\tilde{\mathbf{A}}_{in} = (\tilde{a}_{in,1}, \dots)^T$, and S is the coupling matrix ($S_{j,j'} = t_{\min(j,j')}\delta_{j,j'\pm 1}$). The coupling matrix is Hermitian now and can be diagonalized as

$$S = PJP^{-1}. \quad (\text{C4})$$

$P = (\alpha_1, \alpha_2, \dots)$ and the column vectors α_j are the eigenvectors of S . The diagonal elements of the diagonal matrix $J = \text{Diag}(\lambda_1, \lambda_2, \dots)$ are the corresponding eigenvalues. Then we can rewrite the quantum Langevin equations as

$$\frac{d}{dt}(P^{-1}\tilde{\mathbf{A}}) = \left(-\frac{\kappa}{2}\mathbb{1} - iJ\right)P^{-1}\tilde{\mathbf{A}} - \sqrt{\kappa}P^{-1}\tilde{\mathbf{A}}_{in}. \quad (\text{C5})$$

The time-dependent solution is

$$P^{-1}\tilde{\mathbf{A}}(t) = P^{-1}\tilde{\mathbf{A}}(0)e^{(-\frac{\kappa}{2}\mathbb{1} - iJ)t} + \sqrt{\kappa}\int_0^t e^{(-\frac{\kappa}{2}\mathbb{1} - iJ)(t-t')}P^{-1}\tilde{\mathbf{A}}_{in}(t')dt'. \quad (\text{C6})$$

The stationary solution is

$$\tilde{\mathbf{A}}'_s = \sqrt{\kappa}P \lim_{t \rightarrow \infty} \int_0^t e^{(-\frac{\kappa}{2}\mathbb{1} - iJ)(t-t')}P^{-1}\tilde{\mathbf{A}}_{in}(t')dt' = \sqrt{\kappa} \sum_j \lim_{t \rightarrow \infty} \int_0^t e^{(-\frac{\kappa}{2} - i\lambda_j)(t-t')} [\tilde{\alpha}_j \cdot \tilde{\mathbf{A}}_{in}(t')] \tilde{\alpha}_j dt' \quad (\text{C7})$$

or

$$\tilde{a}_{m,s} = \sqrt{\kappa} \sum_{j,k} \lim_{t \rightarrow \infty} \int_0^t e^{(-\frac{\kappa}{2} - i\lambda_j)(t-t')} \alpha_{j,k} \alpha_{j,m} \tilde{a}_{in,k}(t') dt'. \quad (\text{C8})$$

The noise operators before the squeezing transformation satisfy

$$\langle a_{in,j}(t) a_{in,j}^\dagger(t') \rangle = (n_{th} + 1) \delta(t - t'), \quad (\text{C9})$$

$$\langle a_{in,j}^\dagger(t) a_{in,j}(t') \rangle = \delta(t - t'), \quad (\text{C10})$$

and the noise operators after the squeezing transformation satisfy

$$\langle \tilde{a}_{in,j}(t) \tilde{a}_{in,j}^\dagger(t') \rangle = \delta(t - t') \frac{(e^{2r_j} + e^{-2r_j})(2n_{th} + 1) + 2}{4}, \quad (\text{C11})$$

$$\langle \tilde{a}_{in,j}^\dagger(t) \tilde{a}_{in,j}(t') \rangle = \delta(t - t') \frac{(e^{2r_j} + e^{-2r_j})(2n_{th} + 1) - 2}{4}, \quad (\text{C12})$$

$$\langle \tilde{a}_{in,j}(t) \tilde{a}_{in,j}(t') \rangle = \delta(t - t') \frac{e^{2r_j} - e^{-2r_j}}{4} (2n_{th} + 1). \quad (\text{C13})$$

So the stationary mean values of the second-order moments can be obtained as

$$\begin{aligned} \langle \tilde{a}_m \tilde{a}_{m'} \rangle_s &= \kappa \sum_{j,k,j',k'} \lim_{t \rightarrow \infty} \int_0^t dt' \int_0^t dt'' e^{(-\kappa/2 - i\lambda_j)(t-t')} \alpha_{j,k} \alpha_{j,m} e^{(-\kappa/2 - i\lambda_{j'}) (t-t'')} \alpha_{j',k'} \alpha_{j',m'} \langle \tilde{a}_{in,k}(t') \tilde{a}_{in,k'}(t'') \rangle \\ &= \kappa \sum_{j,k,j'} \lim_{t \rightarrow \infty} \int_0^t dt' e^{[-\kappa - i(\lambda_j + \lambda_{j'})](t-t')} \alpha_{j,k} \alpha_{j,m} \alpha_{j',k} \alpha_{j',m'} \frac{e^{2r_k} - e^{-2r_k}}{4} (2n_{th} + 1) \\ &= \kappa \sum_{j,k,j'} \frac{1}{\kappa + i(\lambda_j + \lambda_{j'})} \alpha_{j,k} \alpha_{j,m} \alpha_{j',k} \alpha_{j',m'} \frac{e^{2r_k} - e^{-2r_k}}{4} (2n_{th} + 1), \end{aligned} \quad (\text{C14})$$

and similarly

$$\langle \tilde{a}_m^\dagger \tilde{a}_{m'}^\dagger \rangle_s = \kappa \sum_{j,k,j'} \frac{1}{\kappa + i(-\lambda_j^* + \lambda_{j'})} \alpha_{j,k} \alpha_{j,m} \alpha_{j',k} \alpha_{j',m'} \frac{(e^{2r_k} + e^{-2r_k})(2n_{th} + 1) - 2}{4}. \quad (\text{C15})$$

- [1] R. Horodecki, P. Horodecki, M. Horodecki, and K. Horodecki, Quantum entanglement, *Rev. Mod. Phys.* **81**, 865 (2009).
- [2] L. Pezzè, A. Smerzi, M. K. Oberthaler, R. Schmied, and P. Treutlein, Quantum metrology with nonclassical states of atomic ensembles, *Rev. Mod. Phys.* **90**, 035005 (2018).
- [3] A. Einstein, B. Podolsky, and N. Rosen, Can quantum-mechanical description of physical reality be considered complete? *Phys. Rev.* **47**, 777 (1935).
- [4] P. Colciaghi, Y. Li, P. Treutlein, and T. Zibold, Einstein-podolsky-rosen experiment with two bose-einstein condensates, *Phys. Rev. X* **13**, 021031 (2023).
- [5] F. Arute, K. Arya, R. Babbush, D. Bacon, J. C. Bardin, R. Barends, R. Biswas, S. Boixo, F. G. S. L. Brandao, D. A. Buell *et al.*, Quantum supremacy using a programmable superconducting processor, *Nature (London)* **574**, 505 (2019).
- [6] H.-S. Zhong, H. Wang, Y.-H. Deng, M.-C. Chen, L.-C. Peng, Y.-H. Luo, J. Qin, D. Wu, X. Ding, Y. Hu *et al.*, Quantum computational advantage using photons, *Science* **370**, 1460 (2020).
- [7] Y. Wu, W.-S. Bao, S. Cao, F. Chen, M.-C. Chen, X. Chen, T.-H. Chung, H. Deng, Y. Du, D. Fan *et al.*, Strong quantum computational advantage using a superconducting quantum processor, *Phys. Rev. Lett.* **127**, 180501 (2021).
- [8] L. Pezzè and A. Smerzi, Entanglement, nonlinear dynamics, and the heisenberg limit, *Phys. Rev. Lett.* **102**, 100401 (2009).
- [9] C. Gross, T. Zibold, E. Nicklas, J. Estève, and M. K. Oberthaler, Nonlinear atom interferometer surpasses classical precision limit, *Nature (London)* **464**, 1165 (2010).
- [10] M. F. Riedel, P. Böhi, Y. Li, T. W. Hänsch, A. Sinatra, and P. Treutlein, Atom-chip-based generation of entanglement for quantum metrology, *Nature (London)* **464**, 1170 (2010).
- [11] X.-Y. Luo, Y.-Q. Zou, L.-N. Wu, Q. Liu, M.-F. Han, M. K. Tey, and L. You, Deterministic entanglement generation from driving through quantum phase transitions, *Science* **355**, 620 (2017).
- [12] O. Hosten, N. J. Engelsen, R. Krishnakumar, and M. A. Kasevich, Measurement noise 100 times lower than the quantum-projection limit using entangled atoms, *Nature (London)* **529**, 505 (2016).
- [13] Y.-Q. Zou, L.-N. Wu, Q. Liu, X.-Y. Luo, S.-F. Guo, J.-H. Cao, M. K. Tey, and L. You, Beating the classical precision limit with spin-1 Dicke states of more than 10,000 atoms, *Proc. Natl. Acad. Sci. USA* **115**, 6381 (2018).
- [14] E. Pedrozo-Peñañiel, S. Colombo, C. Shu, A. F. Adiyatullin, Z. Li, E. Mendez, B. Braverman, A. Kawasaki, D. Akamatsu, Y. Xiao, and V. Vuletić, Entanglement on an optical atomic-clock transition, *Nature (London)* **588**, 414 (2020).
- [15] Q. Liu, L.-N. Wu, J.-H. Cao, T.-W. Mao, X.-W. Li, S.-F. Guo, M. K. Tey, and L. You, Nonlinear interferometry beyond classical limit enabled by cyclic dynamics, *Nat. Phys.* **18**, 167 (2022).
- [16] S. Wu, G. Bao, J. Guo, J. Chen, W. Du, M. Shi, P. Yang, L. Chen, and W. Zhang, Quantum magnetic gradiometer with entangled twin light beams, *Sci. Adv.* **9**, eadg1760 (2023).
- [17] X.-G. Wen, Colloquium: Zoo of quantum-topological phases of matter, *Rev. Mod. Phys.* **89**, 041004 (2017).
- [18] H. M. Price, O. Zilberberg, T. Ozawa, I. Carusotto, and N. Goldman, Four-dimensional quantum Hall effect with ultracold atoms, *Phys. Rev. Lett.* **115**, 195303 (2015).
- [19] H. M. Price, T. Ozawa, and N. Goldman, Synthetic dimensions for cold atoms from shaking a harmonic trap, *Phys. Rev. A* **95**, 023607 (2017).
- [20] L. Taddia, E. Cornfeld, D. Rossini, L. Mazza, E. Sela, and R. Fazio, Topological fractional pumping with Alkaline-earth-like atoms in synthetic lattices, *Phys. Rev. Lett.* **118**, 230402 (2017).
- [21] S. Sugawa, F. Salces-Carcoba, A. R. Perry, Y. Yue, and I. B. Spielman, Second Chern number of a quantum-simulated non-Abelian Yang monopole, *Science* **360**, 1429 (2018).
- [22] T. Chalopin, T. Satoor, A. Evrard, V. Makhlov, J. Dalibard, R. Lopes, and S. Nascimbene, Probing chiral edge dynamics and bulk topology of a synthetic Hall system, *Nat. Phys.* **16**, 1017 (2020).
- [23] Z.-Y. Wang, X.-C. Cheng, B.-Z. Wang, J.-Y. Zhang, Y.-H. Lu, C.-R. Yi, S. Niu, Y. Deng, X.-J. Liu, S. Chen, and J.-W. Pan, Realization of an ideal Weyl semimetal band in a quantum gas with 3D spin-orbit coupling, *Science* **372**, 271 (2021).
- [24] X.-Q. Wang, G.-Q. Luo, J.-Y. Liu, W. V. Liu, A. Hemmerich, and Z.-F. Xu, Evidence for an atomic chiral superfluid with topological excitations, *Nature (London)* **596**, 227 (2021).
- [25] F. D. M. Haldane, Model for a quantum Hall effect without Landau levels: Condensed-matter realization of the “Parity Anomaly”, *Phys. Rev. Lett.* **61**, 2015 (1988).
- [26] L. Lu, J. D. Joannopoulos, and M. Soljačić, Topological photonics, *Nat. Photonics* **8**, 821 (2014).
- [27] Y. Yang, Z. Gao, H. Xue, L. Zhang, M. He, Z. Yang, R. Singh, Y. Chong, B. Zhang, and H. Chen, Realization of a three-dimensional photonic topological insulator, *Nature (London)* **565**, 622 (2019).
- [28] A. El Hassan, F. K. Kunst, A. Moritz, G. Andler, E. J. Bergholtz, and M. Bourennane, Corner states of light in photonic waveguides, *Nat. Photonics* **13**, 697 (2019).
- [29] M. Li, D. Zhirihin, M. Gorlach, X. Ni, D. Filonov, A. Slobozhanyuk, A. Alù, and A. B. Khanikaev, Higher-order topological states in photonic kagome crystals with long-range interactions, *Nat. Photonics* **14**, 89 (2020).
- [30] Y. Ao, X. Hu, Y. You, C. Lu, Y. Fu, X. Wang, and Q. Gong, Topological phase transition in the non-Hermitian coupled resonator array, *Phys. Rev. Lett.* **125**, 013902 (2020).
- [31] S. Xia, D. Kaltsas, D. Song, I. Komis, J. Xu, A. Szameit, H. Buljan, K. G. Makris, and Z. Chen, Nonlinear tuning of PT symmetry and non-Hermitian topological states, *Science* **372**, 72 (2021).
- [32] E. Lustig, L. J. Maczewsky, J. Beck, T. Biesenthal, M. Heinrich, Z. Yang, Y. Plotnik, A. Szameit, and M. Segev, Photonic topological insulator induced by a dislocation in three dimensions, *Nature (London)* **609**, 931 (2022).
- [33] T. Ozawa, H. M. Price, A. Amo, N. Goldman, M. Hafezi, L. Lu, M. C. Rechtsman, D. Schuster, J. Simon, O. Zilberberg, and I. Carusotto, Topological photonics, *Rev. Mod. Phys.* **91**, 015006 (2019).
- [34] J. H. P. Colpa, Diagonalization of the quadratic boson hamiltonian, *Phys. A (Amsterdam)* **93**, 327 (1978).
- [35] D. Vitali, S. Gigan, A. Ferreira, H. R. Böhm, P. Tombesi, A. Guerreiro, V. Vedral, A. Zeilinger, and M. Aspelmeyer, Optomechanical entanglement between a movable mirror and a cavity field, *Phys. Rev. Lett.* **98**, 030405 (2007).
- [36] L. Tian, Robust photon entanglement via quantum interference in optomechanical interfaces, *Phys. Rev. Lett.* **110**, 233602 (2013).
- [37] Y.-D. Wang and A. A. Clerk, Reservoir-engineered entanglement in optomechanical systems, *Phys. Rev. Lett.* **110**, 253601 (2013).

- [38] S. Mittal, E. A. Goldschmidt, and M. Hafezi, A topological source of quantum light, *Nature (London)* **561**, 502 (2018).
- [39] M. Esposito, A. Ranadive, L. Planat, S. Leger, D. Fraudet, V. Jouanny, O. Buisson, W. Guichard, C. Naud, J. Aumentado, F. Lecocq, and N. Roch, Observation of two-mode squeezing in a traveling wave parametric amplifier, *Phys. Rev. Lett.* **128**, 153603 (2022).
- [40] B.-U. Sohn, Y.-X. Huang, J. W. Choi, G. F. R. Chen, D. K. T. Ng, S. A. Yang, and D. T. H. Tan, A topological nonlinear parametric amplifier, *Nat. Commun.* **13**, 7218 (2022).
- [41] O. Morsch and M. Oberthaler, Dynamics of bose-einstein condensates in optical lattices, *Rev. Mod. Phys.* **78**, 179 (2006).
- [42] L. Fallani, L. De Sarlo, J. E. Lye, M. Modugno, R. Saers, C. Fort, and M. Inguscio, Observation of dynamical instability for a Bose-Einstein condensate in a moving 1d optical lattice, *Phys. Rev. Lett.* **93**, 140406 (2004).
- [43] T. Boulier, J. Maslek, M. Bukov, C. Bracamontes, E. Magnan, S. Lellouch, E. Demler, N. Goldman, and J. V. Porto, Parametric heating in a 2d periodically driven bosonic system: Beyond the weakly interacting regime, *Phys. Rev. X* **9**, 011047 (2019).
- [44] K. Wintersperger, M. Bukov, J. Näger, S. Lellouch, E. Demler, U. Schneider, I. Bloch, N. Goldman, and M. Aidelsburger, Parametric instabilities of interacting bosons in periodically driven 1d optical lattices, *Phys. Rev. X* **10**, 011030 (2020).
- [45] M. Aspelmeyer, T. J. Kippenberg, and F. Marquardt, Cavity optomechanics, *Rev. Mod. Phys.* **86**, 1391 (2014).
- [46] H.-K. Li, X.-X. Ren, Y.-C. Liu, and Y.-F. Xiao, Photon-photon interactions in a largely detuned optomechanical cavity, *Phys. Rev. A* **88**, 053850 (2013).
- [47] A. McDonald, T. Pereg-Barnea, and A. A. Clerk, Phase-dependent chiral transport and effective non-Hermitian dynamics in a Bosonic Kitaev-Majorana chain, *Phys. Rev. X* **8**, 041031 (2018).
- [48] K. Yokomizo and S. Murakami, Non-Bloch band theory in bosonic Bogoliubov-de Gennes systems, *Phys. Rev. B* **103**, 165123 (2021).
- [49] J. del Pino, J. J. Slim, and E. Verhagen, Non-Hermitian chiral phononics through optomechanically induced squeezing, *Nature (London)* **606**, 82 (2022).
- [50] Q. Wang, C. Zhu, Y. Wang, B. Zhang, and Y. D. Chong, Amplification of quantum signals by the non-Hermitian skin effect, *Phys. Rev. B* **106**, 024301 (2022).
- [51] V. P. Flynn, E. Cobanera, and L. Viola, Topology by dissipation: Majorana bosons in metastable quadratic Markovian dynamics, *Phys. Rev. Lett.* **127**, 245701 (2021).
- [52] A. Pocklington, Y.-X. Wang, and A. A. Clerk, Dissipative pairing interactions: Quantum instabilities, topological light, and volume-law entanglement, *Phys. Rev. Lett.* **130**, 123602 (2023).
- [53] L.-L. Wan and X.-Y. Lü, Quantum-squeezing-induced point-gap topology and skin effect, *Phys. Rev. Lett.* **130**, 203605 (2023).
- [54] W. P. Su, J. R. Schrieffer, and A. J. Heeger, Solitons in polyacetylene, *Phys. Rev. Lett.* **42**, 1698 (1979).
- [55] W. P. Su, J. R. Schrieffer, and A. J. Heeger, Soliton excitations in polyacetylene, *Phys. Rev. B* **22**, 2099 (1980).
- [56] Y.-C. Liu, Y.-F. Xiao, X. Luan, and C. W. Wong, Dynamic dissipative cooling of a mechanical resonator in strong coupling optomechanics, *Phys. Rev. Lett.* **110**, 153606 (2013).
- [57] G. Vidal and R. F. Werner, Computable measure of entanglement, *Phys. Rev. A* **65**, 032314 (2002).
- [58] J. K. Asbóth, L. Oroszlány, and A. Pályi, *A Short Course on Topological Insulators*, Lecture Notes in Physics (Springer, Cham, 2016), Vol. 919.
- [59] M. C. Rechtsman, Y. Lumer, Y. Plotnik, A. Perez-Leija, A. Szameit, and M. Segev, Topological protection of photonic path entanglement, *Optica* **3**, 925 (2016).
- [60] A. Blanco-Redondo, B. Bell, D. Oren, B. J. Eggleton, and M. Segev, Topological protection of biphoton states, *Science* **362**, 568 (2018).
- [61] Y. Wang, Y.-H. Lu, J. Gao, R.-J. Ren, Y.-J. Chang, Z.-Q. Jiao, Z.-Y. Zhang, and X.-M. Jin, Topologically protected quantum entanglement, [arXiv:1903.03015](https://arxiv.org/abs/1903.03015).
- [62] K. Tschernig, Á. Jimenez-Galán, D. N. Christodoulides, M. Ivanov, K. Busch, M. A. Bandres, and A. Perez-Leija, Topological protection versus degree of entanglement of two-photon light in photonic topological insulators, *Nat. Commun.* **12**, 1974 (2021).
- [63] Y. Wang, X.-L. Pang, Y.-H. Lu, J. Gao, Y.-J. Chang, L.-F. Qiao, Z.-Q. Jiao, H. Tang, and X.-M. Jin, Topological protection of two-photon quantum correlation on a photonic chip, *Optica* **6**, 955 (2019).
- [64] M. Wang, C. Doyle, B. Bell, M. J. Collins, E. Magi, B. J. Eggleton, M. Segev, and A. Blanco-Redondo, Topologically protected entangled photonic states, *Nanophotonics* **8**, 1327 (2019).
- [65] T. Dai, Y. Ao, J. Bao, J. Mao, Y. Chi, Z. Fu, Y. You, X. Chen, C. Zhai, B. Tang, Y. Yang, Z. Li, L. Yuan, F. Gao, X. Lin, M. G. Thompson, J. L. O'Brien, Y. Li, X. Hu, Q. Gong *et al.*, Topologically protected quantum entanglement emitters, *Nat. Photonics* **16**, 248 (2022).
- [66] R.-J. Ren, Y.-H. Lu, Z.-K. Jiang, J. Gao, W.-H. Zhou, Y. Wang, Z.-Q. Jiao, X.-W. Wang, A. S. Solntsev, and X.-M. Jin, Topologically protecting squeezed light on a photonic chip, *Photon. Res.* **10**, 456 (2022).
- [67] V. Peano, M. Houde, C. Brendel, F. Marquardt, and A. A. Clerk, Topological phase transitions and chiral inelastic transport induced by the squeezing of light, *Nat. Commun.* **7**, 10779 (2016).
- [68] H. Cai and D.-W. Wang, Topological phases of quantized light, *Natl. Sci. Rev.* **8**, nwaal196 (2021).
- [69] J. Deng, H. Dong, C. Zhang, Y. Wu, J. Yuan, X. Zhu, F. Jin, H. Li, Z. Wang, H. Cai, C. Song, H. Wang, J. Q. You, and D.-W. Wang, Observing the quantum topology of light, *Science* **378**, 966 (2022).